Observation of a Chiral-Symmetry-Breaking Twist-Bend Instability in Achiral Freely Suspended Liquid-Crystal Films

Jinzhong Pang and Noel A. Clark
Department of Physics, University of Colorado, Boulder, Colorado 80309
(Received 10 June 1994)

Freely suspended smectic-C films, 2, 3, and 4 layers in thickness, of the achiral compound $C_7F_{15}CH_2O$-ϕ-COO-ϕ-OC_6H_{13} exhibit a thermotropic transition at which the uniform two-dimensional smectic-C molecular orientation field becomes modulated by a periodic bend wave soliton. No such transition is found in single-layer films. This transition is interpreted as a chiral-symmetry-breaking transition, marking the spontaneous appearance of frustrated local bend.

PACS numbers: 61.30.Jf

Some of the most interesting structures of liquid-crystal phases arise as a result of internal frustration, the situation in which the local energetically ideal configuration cannot be extended to fill space, but must be accommodated by the appearance of defects, often in periodic arrays [1]. The classic 3D examples are the blue phases, in which the optimal filling of space with the symmetry-imposed 2D twist of the local average molecular long axis orientation $\mathbf{n}(\mathbf{r})$ requires a network of line or point defects [2]. Such frustration-induced modulations are also found at the smectic-C–air interface in thermotropic freely suspended films [3,4], and, recently, in Langmuir monolayers [5], in the form of a quasiperiodic modulation of $\mathbf{c}(x,y)$ giving the projection of $\mathbf{n}(\mathbf{r})$ at the surface onto the surface plane. In these cases the head-tail polar molecular ordering at the surface induces a preference for nonzero splay of $\mathbf{n}(\mathbf{r})$ and, in turn, of $\mathbf{c}(x,y)$, giving rise to the splay stripes which enable the preferred sign of splay everywhere on the surface [6]. Similarly, stripes having one sign of bend appear in freely suspended liquid crystal films as a result molecular chirality [7,8].

In these examples it is the intrinsic symmetry that favors local splay, bend, or twist of a particular sign. In this Letter we report the first observation of internal frustration and consequent spatial modulation appearing as a spontaneously broken symmetry, initially in the form of a bend wave in $\mathbf{c}(x,y)$ of a smectic C. These structures are readily distinguished from the above examples in that while this system locally prefers bend there is *no preference as to the sign of the bend,* so that both signs appear equivalently. The possibility of such an instability was recently shown using a theoretical model based on a Landau free energy by Selinger, Wang, Bruinsma, and Knobler (SWBK), who calculated a phase diagram having regions of 1D and 2D sinusoidal and solitonlike modulations [9]. They also point out that, since in the smectic-C phase local bend implies local twist and therefore local chirality, this bend instability is a periodic chiral symmetry breaking. Here, we present clear evidence for such a thermotropic spontaneous chiral-symmetry-breaking transition in an achiral smectic-C material.

Experiments were carried out on 1- to 10-layer thick freely suspended films of the achiral 3M compound CRL-EX-900084 ($C_7F_{15}CH_2O$-ϕ-COO-ϕ-OC_6H_{13}), notable for having one aliphatic and one perfluoroalkyl chain. The bulk material has isotropic (I), smectic-A (Sm-A), smectic-C (Sm-C), and crystal (K) phases vs temperature T as follows $I \xrightarrow{136}$ Sm-A $\xrightarrow{79}$ Sm-C $\xrightarrow{71}$ K. In 1- to 4-layer thick freely suspended films the crystallization transition is suppressed below 71 °C and the smectic-C can be observed to lower T. As T is decreased the films eventually break, with $T = 65$ °C the lowest achieved in a liquid-crystal phase. The film geometry is shown in Fig. 1(a). The local mean molecular long axis, given by the director $\mathbf{n}$, is tilted relative to the layer and film plane normal through an equilibrium angle θ [10]. The projection direction of $\mathbf{n}(x,y)$ onto the film plane defines the 2D "$\mathbf{c}$ director" unit vector field $\mathbf{c}(x,y)$, shown in Fig. 1(a), having a *local mean* scalar azimuthal orientation $\phi(x,y)$ which can be visualized using depolarized reflected light microscopy (DRLM) [11,12]. Films were drawn over a 3 × 10 mm hole in a glass cover slip in a

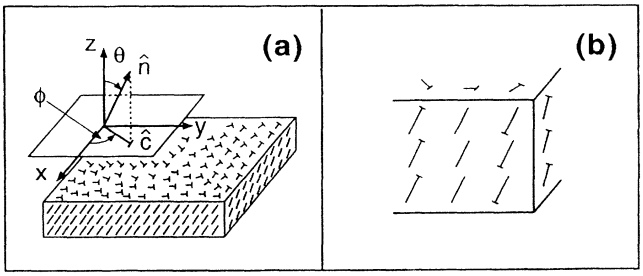

FIG. 1. (a) Freely suspended smectic-C film geometry. The mean molecular long axis orientation is described by a vector $\mathbf{n}(\mathbf{r})$ with a fixed tilt angle θ from layer normal. The "$\mathbf{c}$ director," $\mathbf{c}(x,y)$, the unit vector giving the projection of $\mathbf{n}(\mathbf{r})$ on layer plane, has a variable azimuthal orientation $\phi(x,y)$. The "tees" give the projection of $\mathbf{n}$ on the surfaces indicated, with the small bar on the end of the molecule closest to the surface. (b) Geometry showing that bend of $\mathbf{c}(x,y)$ requires both twist and bend of $\mathbf{n}(\mathbf{r})$ and that when θ is small the principal deformation of $\mathbf{n}$ is twist.

 0031-9007/94/73(17)/2332(4)$06.00

hot stage closed with tilted double windows on the top and bottom to minimize internal thermal gradients and give 0.01 K temperature stability. Because the liquid crystal molecules are optically anisotropic, the polarization vector for light reflected from a film will be rotated a few degrees toward $\mathbf{c}$ relative to the incident-light polarization [11]. The film image in DRLM is thus marked by dark brushes where $\mathbf{c}$ is parallel or normal to the incident polarization and by bright brushes when $\mathbf{c}$ is at the intermediate $(\pi/4)$ orientations [11]. Here we use oblique incidence and a slight uncrossing of the analyzer [12] to *uniquely* map $\mathbf{c}(x, y)$.

Figures 2(a)–2(d) show DRLM images of the instability as it appears upon lowering temperature in the Sm-C phase of a 4-layer thick film. The Sm-A to Sm-C transition is at 85 °C in the 4-layer film (the Sm-A–Sm-C transition is elevated in thin films as is usual [13]) and the Sm-C texture obtained is typical for freely suspended smectic-C films: a gradual variation of $\mathbf{c}(x, y)$ across the film, marked by the dramatic flickering due to orientational fluctuations of $\mathbf{c}$ [10,11]. At $T = 70.4$ °C batonnetlike regions of spontaneous deformation of $\mathbf{c}(x, y)$, shown in Fig. 2(a), nucleate at many places on the film [~10 in Fig. 2(a)] and gradually grow to cover it. The boxed area of the batonnet growing tip is mapped in Fig. 3(a). As T is further lowered the deformation evolves into a quasiperiodic network of stringlike line defects, as shown in Fig. 2(b) at $T =$ 70.0 °C. This local quasiperiodicity enforces a 2D focal coniclike texture on larger length scales. The string defect spacing decreases with decreasing T, ultimately falling below ~5 μm, the resolution of the microscope, and in this limit the 2D focal coniclike texture, shown at $T =$ 69.0 °C in Fig. 2(c) for a 4-layer film, and in Fig. 2(d) at $T = 71$ °C for a 2-layer film, can be visualized, because of the anisotropy in the local mean orientation of $\mathbf{c}$ relative to the local stripes. These focal conic textures bear a strong resemblance to the global textures found in other 2D systems having local periodicity [14,15].

Since the bend of $\mathbf{c}$ removes the $\mathbf{z}$-$\mathbf{c}$ mirror symmetry plane, it leaves the film locally with only a C_2 axis along $\mathbf{p} = \mathbf{c} \times \mathbf{z}$. Thus, the bend wave produces a local chiral symmetry breaking of the initially achiral system, and there is a local ferroelectric polarization $\mathbf{P} = \beta[\mathbf{c} \times \nabla \times \mathbf{c}]$, along $\mathbf{p}$, where β is a constant of proportionality. Also, a necessary consequence of the chiral symmetry breaking is the twist of $\mathbf{n}(x, y, z)$ which accompanies the bend of $\mathbf{c}(x, y)$, or, as we suggest below, may drive it.

Figure 3(a) shows a DRLM mapping of the structure of $\mathbf{c}(x, y)$ in the vicinity of a growing tip of a batonnet of the instability in a 4-layer film [boxed area of Fig. 2(a)]. The principal distortion when the instability first appears is a periodic *bend* modulation of $\mathbf{c}(x, y)$, the film developing regions of nonzero $\nabla \times \mathbf{c}$, which periodically changes sign in a 1D wavelike pattern. The regions of opposite sign of bend initially occur equivalently, the instability appearing to simply favor finite bend, without selection with respect to its sign. *It is important to note that all of these changes occur within the smectic-C phase, that is, there is no evidence that they are a result of transitions to more ordered smectic-F, -I, or -L phases.* As the batonnet grows, the bend modulation increases in amplitude, developing into distinct stripes having a boundary line, shown as the solid line in Fig. 3(a), at which the *sign* of bend abruptly changes, i.e., at which the bend amplitude evolves from a "sinusoidal" to a "square wave" solitonlike periodic spatial dependence. Note that $\mathbf{c}(x, y)$

FIG. 2. DRLM photomicrographs of CRL-EX-900084 freely suspended smectic-C films. The diameter of the field is zz μm on the film: (a) Batonnets (~10) of the bend instability appearing in the smectic-C phase in a 4-layer film at $T = 70.4$ °C. The growing batonnet tip (box) is mapped in Fig. 3(a). (b) Quasiperiodic network of stringlike line defects, developing at $T = 70.0$ °C out of the batonnets in a 4-layer film. The defect textures are characteristic of those found in 2D periodic stripe systems [14,15]. (c) Global 2D focal conic texture obtained in a 4-layer film at $T = 69$ °C where the local period has decreased to below the microscope resolution. Here DRLM visualizes the local stripe orientation because of the anisotropy in the average orientation of $\mathbf{c}$ relative to the strings. The boxed area is mapped in Fig. 3. (d) Global texture obtained in a 2-layer film at $T = 69$ °C. This texture is found in other 2D periodic stripe systems [14,15].

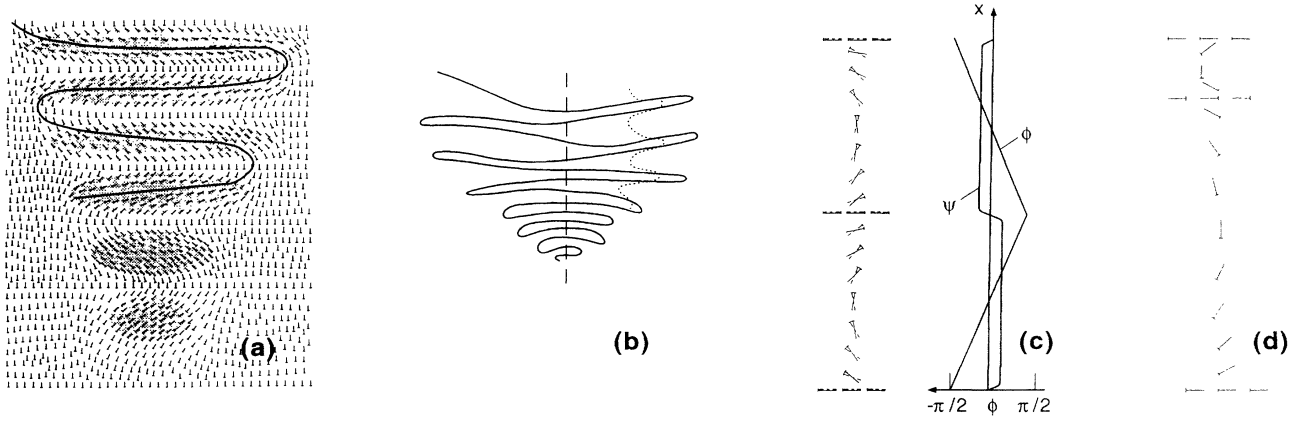

FIG. 3. (a) DRLM map of the growing batonnet tip of Fig. 2(a), showing that the instability is a bend wave, with positive and negative bend appearing equivalently. The fully developed instability, further into the batonnet, is solitonlike [9], a periodic array formed by a line defect where $\mathbf{c}$ is continuous (zero strength strings [12]) and the sign of bend switches. (b) Typical geometry of the bend soliton line (zero strength string [12]) in a growing batonnet. The dotted line indicates a contour of $\mathbf{c}$. While the two signs of bend are of similar strength along the (dashed) batonnet center line, positive bend becomes larger on the right-hand side of the batonnet and vice versa, with a ratio of the bend magnitudes as large as 10:1 developing. Overall the net chirality (bend) averages to zero. (c) Schematic of the bend soliton in which positive and negative bend form equivalent structures, showing the associated the twist of $\mathbf{n}$, indicated by the solid and dot-dashed directors of adjacent layers; the position dependence of $\phi(x)$; and the position dependence of the symmetry breaking order parameter $\psi(x)$ [9]. (d) Schematic of the inequivalent bend soliton, evident in (b) and Figs. 2(a) and 2(b).

is locally parallel to the stripe boundary and does not change in orientation as it is crossed, i.e., the boundary line is an "$s = 0$ string," as first identified by Pang, Muzny, and Clark [12], marking *only* the change in preferred sign of bend. Figure 3(b) shows the typical larger scale structure of the bend soliton line in a developing batonnet, and Fig. 3(c) shows the 1D bend soliton structure obtained from the SWBK model along with its corresponding $\phi(x)$. The qualitative match to the observed deformation is very good, with the important exception that maximum magnitude of the bend in the regions of opposite bend sign can be *inequivalent* in the soliton regime. This is evident in Figs. 2(a) and 2(b), especially in the interfacial region between the modulated and uniform phases, and shown schematically in Figs. 3(b) and 3(d). The ratio of maximum bend magnitudes in the regions of opposite sign can be as large as ~10:1. While this indicates a local predominance of one chiral sign, the global average of the chirality appears to be zero, as shown for the batonnet in Fig. 3(b), where the two signs of bend dominate similarly but in different regions. Modification of the SWBK model to account for inequivalent bend is discussed below.

This bend instability is found in 2-, 3-, and 4-layer films. In 5-layer and thicker films crystallization preempts the instability upon lowering T, with elongated crystallites growing out onto the film from the edge before the instability can occur upon lowering temperature. It is possible to make 1-layer films of this material. These remain in the uniform smectic-C texture for $T > 65$ °C. Thus the instability, if it occurs at all in 1-layer films, is strongly suppressed, although, as indicated below, we have good reason to expect that the instability will not be found at all in 1-layer films. The temperatures for the onset of the instability in 1- to 4-layer thick films are $T_1 < 65$ °C, $T_2 = 71.5$ °C, $T_3 = 68.8$ °C, and $T_4 = 70.4$ °C, exhibiting an odd-even oscillation in the onset temperature. The instability exhibits some thermal hysteresis.

The localized batonnetlike nucleation of the instability, the coexistence of unmodulated and modulated phases, and the hysteresis indicate onset behavior analogous to that of a first order phase transition. However, other first order liquid transitions, such as the nematic-isotropic, two phase coexistence [c.f. Figs. 2(a) and 2(b)], and thermal hysteresis, indicate the presence of a low concentration of impurities having different solubility in the unmodulated and modulated phases.

Several qualitative features of this transition can be understood from the extension of the SWBK free energy, generalized to include a concentration variable ρ and a cubic term in the bend distortion:

$$F = \int d^2r \Big\{ \Big[\tfrac{1}{2} K_1 (\nabla \cdot \mathbf{c})^2 + \tfrac{1}{2} K_3 (\nabla \times \mathbf{c})^2 - \lambda \psi (\nabla \times \mathbf{c}) + \tfrac{1}{2} \alpha (\nabla \times \mathbf{c})^3 \Big] + \Big[\tfrac{1}{2} k (\nabla \psi)^2 + \tfrac{1}{2} t \psi^2 + \tfrac{1}{4} m \psi^4 + \tfrac{1}{6} n \psi^6 \Big] + \Big[\tfrac{1}{2} A (\nabla r)^2 + \tfrac{1}{2} B r^2 + C \psi^2 r \Big] \Big\}.$$

Here K_1 and K_3 are the Frank elastic constants for splay and bend, respectively, and λ is the constant that determines the coupling of bend to the symmetry-breaking order parameter ψ. The second term is a Landau free energy which

generates the appearance of ψ. We add the third bracket term which couples a concentration variable ρ to ψ. For $C > 0$ and sufficiently large, the coupling to ρ will drive the transition first order. Since the material is achiral ψ is a pseudoscalar quantity.

Comparing our results to the predictions of the SWBK model [9], we are qualitatively in the region of their phase diagram where sinusoidal stripe, square lattice, and soliton regions are successively encountered upon lowering T. As expected from the model the stripe periodicity decreases with decreasing T, indicating an increasing amplitude of ψ. The model predicts that as T is further decreased an increase and divergence of the periodicity to form a uniform chiral phase, a consequence of the increasing energy cost of spatial gradients of ψ. We do not observe such a divergence, possibly indicating that κ is small, although the T range where the modulated phase is accessible is rather narrow.

The cubic term in $\nabla \times \mathbf{c}$ in F enables stripes of opposite chirality to have different widths under the circumstance that the stripe pattern is under dilative strain, which makes α negative. We find that in our films the stripes form with the largest width observed, and the width then tends to decrease with decreasing T, requiring the addition of new stripes to the pattern. This process may require nucleation or be limited by kinetics, leaving the stripe pattern with a larger average stripe width than equilibrium, and therefore with dilative strain on the stripes. Under this condition we will have $\alpha < 0$, and for $|\alpha|$ sufficiently large the system, rather than having uniformly dilated stripes, will exhibit a period doubling instability, with alternating stripes having nearly the preferred width and the ones in between stretched, as is observed.

We now consider the physical origin of the symmetry breaking in this system. As noted above, bend of $\mathbf{c}(x, y)$ is accompanied by both twist of $\mathbf{n}(\mathbf{r})$, $|\mathbf{n} \cdot \nabla \times \mathbf{n}| = \sin\theta \cos\theta |\nabla \times \mathbf{c}|$, and bend of $\mathbf{n}(\mathbf{r})$, $|\mathbf{n} \times \nabla \times \mathbf{n}| = \sin^2\theta |\nabla \times \mathbf{c}|$. Since the tilt angle $\theta \sim 25°$ is small, the deformation of $\mathbf{n}(\mathbf{r})$ predominantly twist, and, as Fig. 1(b) shows, this twist is largely *intralayer*. The absence of the instability in single layer films then points to an important role for physical differences between layers in single vs multiple layer films. An obvious difference is that the single layer film must be on the average *apolar* with respect to end-for-end molecular orientation, whereas the surface layers in multiple layer films are necessarily polar [16,17]. Further evidence for polar ordering at the surface is found from the surface energy, which is lower for films having even numbers of layers than that of films with odd numbers of layers, indicating a preference for polar surface ordering, a result of the amphiphilic character of this molecule [18].

These observations suggest an instability mechanism favoring twist of $\mathbf{n}(\mathbf{r})$ in polar ordered layers of this material, which we suggest originates as a result of the strong difference of the opposing perfluoro and perhydro alkyl tails. The fluoro tail has a much greater stiffness, owing to the steric hindrance of the fluorine atoms which produces a rigid helical chain, and has a cross-sectional area ~1.27 times that of perhydrogenated one [19]. The polar ordering generates a fluoro-core-hydro trilayer substructure within each smectic layer. The large fluoro chain area and entropic pressure tending to increase the area per molecule in the hydrocarbon tail [20] make this structure have the character of a packing of dumbbell-shaped objects, in which the cores (center regions) can be brought closer together if there is a twist between nearest neighbors.

This work was supported by NSF Solid State Chemistry Grant No. DMR 92-23729. The authors benefited from conversations with J. V. Selinger and C. D. Munzy.

[1] J. M. Carlson, S. A. Langer, and J. P. Sethna, Europhys. Lett. **5**, 327 (1988).
[2] E. Dubois-Violette and B. Pansu, Mol. Cryst. Liq. Cryst. **165**, 151 (1988); P. P. Crooker, Liq. Cryst. **5**, 751 (1989).
[3] R. B. Meyer and P. S. Pershan, Solid State Commun. **13**, 989 (1973).
[4] J. E. Maclennan, Europhys. Lett. **13**, 435 (1990).
[5] J. Ruiz-Garcia, X. Qiu, M.-W. Tsao, G. Marshall, C. M. Knobler, G. A. Overbeck, and D. Mobius, J. Phys. Chem. **97**, 6955 (1993).
[6] J. V. Selinger, in *Complex Fluids,* edited by E. B. Sirota, D. Weitz, T. Witten, and J. Israelchvilli (Materials Research Society, Pittsburgh, 1992), p. 29.
[7] S. A. Langer and J. P. Sethna, Phys. Rev. A **34**, 5035 (1986), see Figs. 2 and 3 photos courtesy of N. A. Clark, D. H. Van Winkle, and C. D. Muzny.
[8] G. A. Hinshaw, Jr., R. G. Petschek, and R. A. Pelkovitz, Phys. Rev. Lett. **60**, 1864 (1988).
[9] J. V. Selinger, J. V. Wang, R. F. Bruinsma, and C. M. Knobler, Phys. Rev. Lett. **70**, 1139 (1993).
[10] C. Y. Young, R. Pindak, N. A. Clark, and R. B. Meyer, Phys. Rev. Lett. **40**, 773 (1978).
[11] R. Pindak, C. Y. Young, R. B. Meyer, and N. A. Clark, Phys. Rev. Lett. **45**, 1193 (1980).
[12] J. Pang, C. D. Munzy, and N. A. Clark, Phys. Rev. Lett. **69**, 2783 (1992).
[13] C. S. Rosenblatt, R. B. Meyer, R. Pindak, and N. A. Clark, Phys. Rev. A **21**, 140 (1980).
[14] M. Seul, R. Monar, L. O'Gorman, and R. Wolfe, Science **254**, 1616 (1991).
[15] M. Seul and R. Wolfe, Phys. Rev. A **46**, 7519 (1992); **46**, 7534 (1992).
[16] T. P. Rieker, G. S. Smith, and E. P. Janulis, in Proceedings of the Fourth International Conference on Ferroelectric Liquid Crystals, Tokyo, Japan, 1993.
[17] J. Hopken and M. Moller, Macromolecules **25**, 2482 (1992).
[18] J. Pang, and N. A. Clark (to be published). These results were obtained from studies of the dynamics of single-layer islands and holes in films of various thickness.
[19] *Polymer Handbook,* edited by J. Brandup and E. H. Immergut (Wiley, New York, 1975).
[20] I. Szleifer, A. Ben-Shaul, and W. M. Gelbart, J. Chem. Phys. **85**, 5345 (1986).

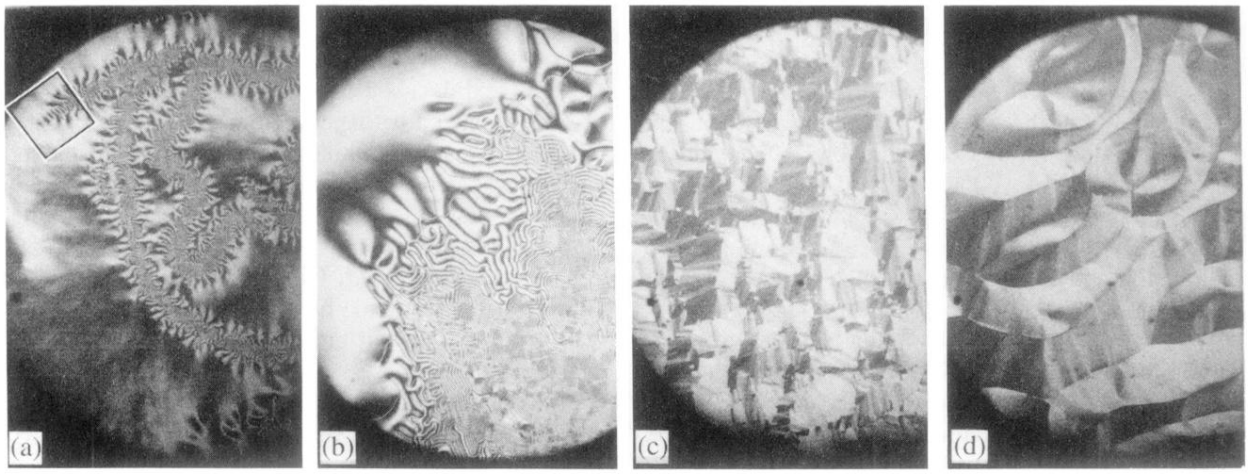

FIG. 2. DRLM photomicrographs of CRL-EX-900084 freely suspended smectic-C films. The diameter of the field is zz μm on the film: (a) Batonnets ($\sim$10) of the bend instability appearing in the smectic-C phase in a 4-layer film at $T = 70.4\,^{\circ}$C. The growing batonnet tip (box) is mapped in Fig. 3(a). (b) Quasiperiodic network of stringlike line defects, developing at $T = 70.0\,^{\circ}$C out of the batonnets in a 4-layer film. The defect textures are characteristic of those found in 2D periodic stripe systems [14,15]. (c) Global 2D focal conic texture obtained in a 4-layer film at $T = 69\,^{\circ}$C where the local period has decreased to below the microscope resolution. Here DRLM visualizes the local stripe orientation because of the anisotropy in the average orientation of $\mathbf{c}$ relative to the strings. The boxed area is mapped in Fig. 3. (d) Global texture obtained in a 2-layer film at $T = 69\,^{\circ}$C. This texture is found in other 2D periodic stripe systems [14,15].

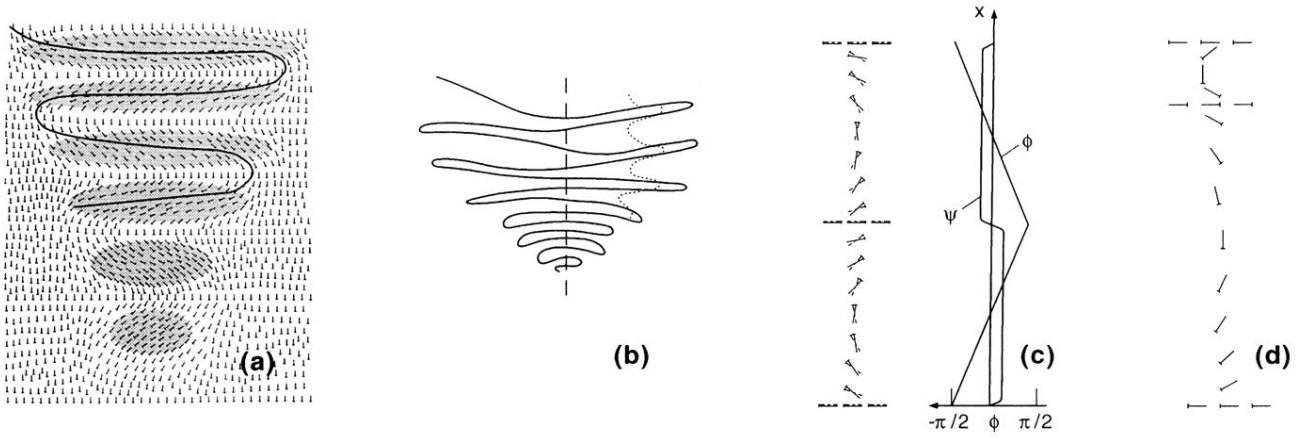

FIG. 3. (a) DRLM map of the growing batonnet tip of Fig. 2(a), showing that the instability is a bend wave, with positive and negative bend appearing equivalently. The fully developed instability, further into the batonnet, is solitonlike [9], a periodic array formed by a line defect where **c** is continuous (zero strength strings [12]) and the sign of bend switches. (b) Typical geometry of the bend soliton line (zero strength string [12]) in a growing batonnet. The dotted line indicates a contour of **c**. While the two signs of bend are of similar strength along the (dashed) batonnet center line, positive bend becomes larger on the right-hand side of the batonnet and vice versa, with a ratio of the bend magnitudes as large as 10:1 developing. Overall the net chirality (bend) averages to zero. (c) Schematic of the bend soliton in which positive and negative bend form equivalent structures, showing the associated the twist of **n**, indicated by the solid and dot-dashed directors of adjacent layers; the position dependence of $\phi(x)$; and the position dependence of the symmetry breaking order parameter $\psi(x)$ [9]. (d) Schematic of the inequivalent bend soliton, evident in (b) and Figs. 2(a) and 2(b).